

Evolution of electronic structure upon Cu doping in the topological insulator Bi_2Se_3

Y. Tanaka,¹ K. Nakayama,¹ S. Souma,² T. Sato,¹ N. Xu,³ P. Zhang,³ P. Richard,³ H. Ding,³ Y. Suzuki,^{4,5} P. Das,^{4,5} K. Kadowaki,^{4,5} and T. Takahashi^{1,2}

¹*Department of Physics, Tohoku University, Sendai 980-8578, Japan*

²*WPI Research Center, Advanced Institute for Materials Research, Tohoku University, Sendai 980-8577, Japan*

³*Beijing National Laboratory for Condensed Matter Physics, and Institute of Physics, Chinese Academy of Sciences, Beijing 100190, China*

⁴*Graduate School of Pure and Applied Sciences, University of Tsukuba, Tsukuba 305-8573, Japan*

⁵*WPI-MANA(NIMS) and CREST-JST*

(Received 10 December 2011; revised manuscript received 20 February 2012; published 12 March 2012)

We have performed angle-resolved photoemission spectroscopy of $\text{Cu}_x\text{Bi}_2\text{Se}_3$ as a function of Cu doping ($x = 0.0\text{--}0.25$) to investigate the doping-induced evolution of the electronic structure. We found that the topological surface state is preserved even in the heavy-doping region ($x = 0.25$), indicative of the robustness of the surface state against doping and impurities. The estimated carrier concentration is far smaller than that expected from a simple intercalation picture, and saturates at $x \sim 0.1$ where superconductivity emerges. This indicates that the carrier concentration responsible for superconductivity is dominated by a subtle balance between two competing processes of electron and hole doping.

DOI: [10.1103/PhysRevB.85.125111](https://doi.org/10.1103/PhysRevB.85.125111)

PACS number(s): 73.20.-r, 71.20.-b, 79.60.-i

I. INTRODUCTION

Three-dimensional topological insulators (3D TIs) are a novel quantum state of matter, where the bulk is an insulator with an energy gap produced by the large spin-orbit coupling, while at the surface an unusual gapless energy dispersion called Dirac cone emerges within the bulk energy gap and is inherently protected by the time reversal symmetry.^{1,2} Owing to the helical spin texture, electrons on the Dirac cone are immune to the backward scattering^{1,3,4} and as a result robust against nonmagnetic impurities and/or disorders,^{5,6} leading to novel quantum properties such as the dissipationless spin transport and the quantum spin Hall effect.⁷ Intensive researches have been carried out to search for new 3D TIs as well as to unveil the mechanism of the peculiar properties. Furthermore, the discovery of 3D TIs triggered the search for a more exotic quantum state of matter, topological superconductor (TSC), which is characterized by a fully gapped odd-parity Cooper pairing and the gapless surface Majorana bound state emerging inside the superconducting gap.^{1,2}

The recent discovery of superconductivity in Cu-doped Bi_2Se_3 ⁸ has stirred fierce debates on the nature of its ground state and whether it provides a platform of topological superconductivity or not.^{8–17} $\text{Cu}_x\text{Bi}_2\text{Se}_3$ starts to show superconductivity at around $x \sim 0.1$ upon Cu doping, with the maximum superconducting transition temperature (T_c) of 3.8 K at $x \sim 0.12$,⁸ and then the T_c value gradually decreases upon further doping, but superconductivity remains even at $x = 0.6$.¹³ Previous angle-resolved photoemission spectroscopy (ARPES) studies^{9,10} have revealed that doped Cu atoms donate electrons into the parent material Bi_2Se_3 to pull down the topological surface state (Dirac cone) with respect to the Fermi level (E_F), but it is still located near E_F even at the optimally doped composition ($x = 0.12$), suggesting that $\text{Cu}_x\text{Bi}_2\text{Se}_3$ provides a suitable platform to study Majorana fermions. While previous ARPES studies have thus made an important step for understanding the key characteristics of doped TIs, there are many unresolved issues yet to be clarified. For instance, the evolution of electronic states in a wider range

of Cu concentration should be investigated to establish the role of Cu doping for superconductivity as well as for the topological surface properties, while the previous studies have been performed in a limited range of concentration ($0.0 \leq x \leq 0.12$). It is also unclear to what extent the topological surface state of superconducting $\text{Cu}_x\text{Bi}_2\text{Se}_3$ is robust against doping beyond $x = 0.12$. These unresolved problems are related to the realization of TI/TSC-based spintronic devices.

In this article, we report a comprehensive ARPES study of $\text{Cu}_x\text{Bi}_2\text{Se}_3$ as a function of Cu doping ($x = 0.0\text{--}0.25$). We found that both the topological surface state and the bulk bands exhibit unusual evolution with Cu doping, and the topological surface state persists in all doping regions without apparent disturbance from the bulk band. We discuss the present experimental result in relation to previous transport and ARPES results, and argue possible ingredients responsible for the occurrence of superconductivity.

II. EXPERIMENTS

High-quality single crystals of $\text{Cu}_x\text{Bi}_2\text{Se}_3$ ($x = 0.0, 0.1, 0.15, 0.25$) were prepared by reacting a pressed pellet of thoroughly mixed powders of Bi(5N), Se(5N), and Cu(4N) in the respective molar ratio in an evacuated quartz tube. The pellet was heated at 1123 K for 24 hours, cooled to 893 K at a rate of 2.5 K/min, and then quenched in liquid nitrogen.¹¹ The actual Cu concentrations in the crystal, as determined by energy-dispersive x-ray (EDX) measurements, are 0.11, 0.13, and 0.22 for the samples with the nominal x values of 0.1, 0.15, and 0.25, respectively. Electron probe microanalysis (EPMA) measurements detected no variation in the Se content upon Cu doping within experimental uncertainties, suggesting that the observed doping evolution of electronic states essentially originates from the Cu-doping effect. X-ray diffraction measurements indicated that the Cu doping causes the monotonic increase of the c -axis length [28.635(15), 28.649(15), 28.658(15), 28.662(15) Å for $x = 0.0, 0.1, 0.15, 0.25$, respectively]. T_c values estimated from

the magnetization measurements for $x = 0.0, 0.1, 0.15$, and 0.25 were $0, 0, 3.28$, and 3.14 K, respectively.

ARPES experiments were carried out with a VG-Scienta R4000 hemispherical analyzer at the U-PGM beam line at Synchrotron Radiation Center (SRC), Wisconsin. All ARPES data have been measured at $T = 30$ K with linearly polarized photons of 17 – 60 eV. The energy and momentum resolutions were set at 15 meV and 0.3° , respectively. We cleaved the sample along the (111) crystal plane in an ultrahigh vacuum better than 3×10^{-11} Torr. ARPES data were recorded within 6 hours after cleaving, time during which we did not observe any signature of surface degradation.

III. RESULTS AND DISCUSSION

We first show ARPES data of pristine Bi_2Se_3 ($x = 0.0$), focusing on the electronic states around the $\bar{\Gamma}$ point of the surface Brillouin zone [see Fig. 1(a)]. The band structure near E_F measured along several momentum (k) cuts in the $k_x - k_z$ plane [see Fig. 1(b)] is displayed in Fig. 1(c). We clearly observe several characteristic features common to all cuts, such as a prominent electronlike band centered at the $\bar{\Gamma}$ point ($k_x = 0$) in the binding energy (E_B) range of 0.0 – 0.3 eV, together with complicated band dispersions at $E_B > 0.3$ eV. The former feature is assigned to the surface state (SS), while the latter one is attributed to the bulk valence bands (VB), since, as seen in Fig. 1(c), the energy position of the former feature is insensitive to the change of photon energy ($h\nu$) in contrast to the latter one. The surface state exhibits an “X”-shaped dispersion, namely Dirac cone, with its Dirac point at 0.23 eV below E_F , indicating that the surface is electron doped. The

highest-lying VB at around 0.4 eV exhibits an “m”-shaped dispersion and approaches closest to E_F at $h\nu = 19$ eV. This photon energy corresponds to the cut in the momentum space which passes through the Γ point in the bulk Brillouin zone (BZ) [see Fig. 1(b)]. At $h\nu = 19$ eV, we also observe a small but finite intensity just below E_F at the Γ point, which is attributed to the bottom of the bulk conduction band (CB). The bulk nature of this band is confirmed by the experimental fact that the spectral intensity vanishes at higher photon energies ($h\nu \geq 23$ eV) due to finite energy dispersion in the k_z direction, indicative of its three dimensionality.

Figure 1(d) shows the ARPES-intensity plot for four samples with different Cu concentrations ($x = 0.0, 0.1, 0.15$, and 0.25) measured at $h\nu = 19$ eV. We used this photon energy to quantitatively estimate the binding energy (E_B) of the CB and VB edges as well as that of the surface state. As seen in Fig. 1(d), all three bands (VB, CB, and surface band) are rigidly shifted downward together upon the Cu doping of $x = 0.1$, as also seen in the energy distribution curves (EDCs) in Fig. 1(e). The Dirac point is distinctly moved from $E_B = 0.23$ eV at $x = 0.0$ to $E_B = 0.45$ eV at $x = 0.1$. However, this downward shift of band dispersion looks to be gradually saturated upon further Cu doping, as seen in the stationary feature of the Dirac point energy ($E_B \sim 0.45$ eV) and the CB bottom ($E_B \sim 0.25$ eV) in the higher doping range ($x = 0.15$ and 0.25). This indicates that doped Cu atoms donate electrons to the parent material Bi_2Se_3 in the early stage of doping up to $x = 0.1$, while the donation is saturated or stopped at $x = 0.1$ – 0.15 , suggesting an anomalous doping process in $\text{Cu}_x\text{Bi}_2\text{Se}_3$. It is also remarked from Fig. 1(d) that the Dirac-cone surface state is clearly seen even at $x = 0.25$ far above the optimal doping level ($x = 0.12$),

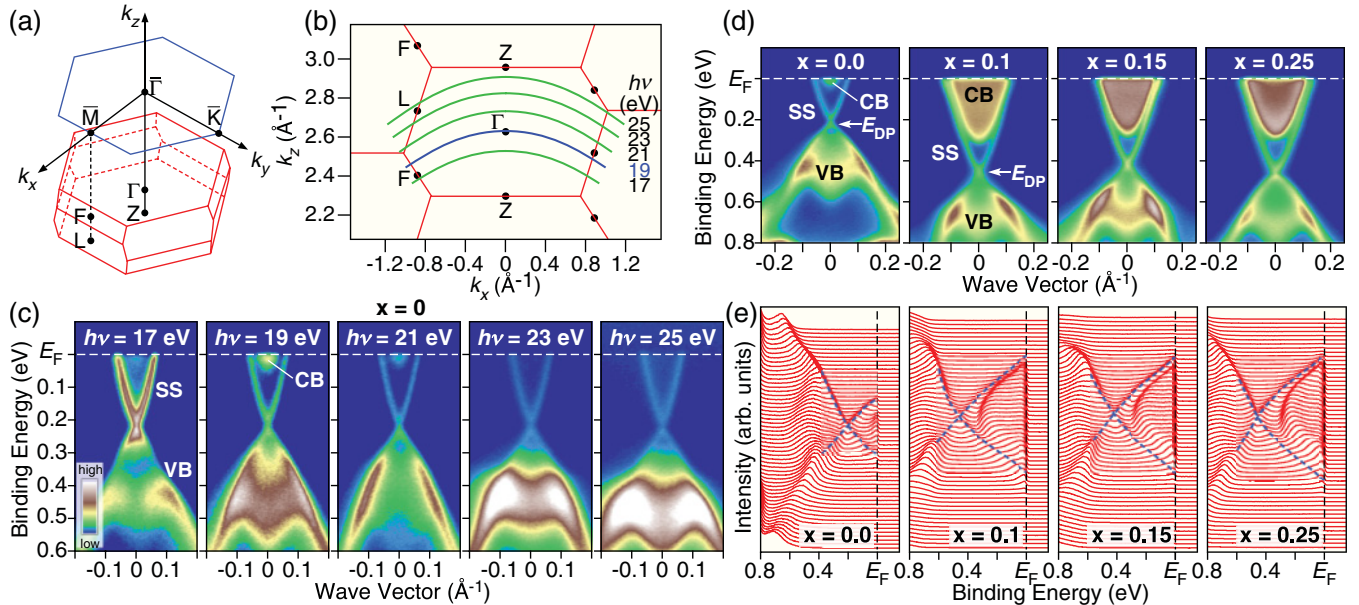


FIG. 1. (Color online) (a) Bulk and surface Brillouin zones (BZs) of $\text{Cu}_x\text{Bi}_2\text{Se}_3$. (b) Bulk BZ in the k_x - k_z plane. (c) Near- E_F ARPES intensity around the $\bar{\Gamma}$ point of pristine Bi_2Se_3 at $T = 30$ K plotted as a function of in-plane wave vector and E_B measured at various k cuts [around the $k_x = 0$ region of the solid curves in (b)]. SS, VB, and CB denote surface state, valence band, and conduction band, respectively. The cut crossing the Γ point of the bulk BZ ($h\nu = 19$ eV) is indicated by a blue curve in (b). We used an inner potential value of $V_0 = 9.7$ eV to calculate the k_z value. (d) and (e) Cu-doping dependence of (d) near- E_F ARPES intensity around the Γ point and (e) corresponding energy distribution curves in $\text{Cu}_x\text{Bi}_2\text{Se}_3$ ($x = 0.0, 0.1, 0.15$, and 0.25) measured at $h\nu = 19$ eV. E_{DP} denotes the energy position of the Dirac point. Blue dashed curves in (e) are a guide to eyes to trace the surface-band dispersions.

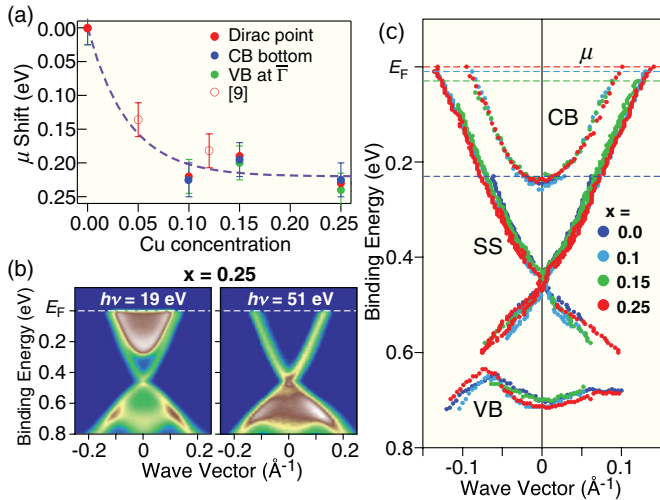


FIG. 2. (Color online) (a) Cu-doping dependence of the chemical potential (μ) shift estimated from the energy shift of the Dirac point (E_{DP}), the conduction-band (CB) bottom, and the valence-band (VB) energy at the Γ point. Previously reported results for E_{DP} ⁹ are also shown for comparison. A purple dashed curve is a guide to eyes to trace the energy shift. (b) Near- E_F ARPES intensity as a function of wave vector and E_B of $\text{Cu}_x\text{Bi}_2\text{Se}_3$ ($x = 0.25$) measured with $h\nu = 19$ and 51 eV. (c) Comparison of the surface-state (SS) and bulk band dispersions in $\text{Cu}_x\text{Bi}_2\text{Se}_3$ ($x = 0.0, 0.1, 0.15, 0.25$) estimated by tracing the peak position in energy distribution curves at $T = 30$ K. The band dispersions are shifted so as to align the Dirac point. The energy position of the chemical potential μ for each composition is shown by a dashed line.

demonstrating that the topological surface state persists even in the heavily-doped region.

Next, we show the chemical-potential (μ) shift as a function of Cu doping. In order to study a possible different μ -shift behavior between surface and bulk, we have evaluated the μ shift with three independent parameters: the Dirac point of surface state (E_{DP}), the CB bottom, and the VB at the Γ point. The first parameter (E_{DP}) would represent the relative shift of the surface states while the latter two are for the bulk. Figure 2(a) shows the experimental result obtained with these three parameters. It is remarked that both shifts and their doping dependence coincide very well with each other for four samples, suggesting that the bulk and surface bands are shifted as a whole with Cu doing in a substantially wide range of doping. It is again noticed here that the μ shift is saturated at $x > 0.1$. In addition to the energy shift of bands, the Cu doping might change the shape of bands. Since the shape of bands near E_F is essential for the physical properties, we compare more precisely the band dispersion as a function of Cu doping in Figs. 2(b) and 2(c). As seen in Fig. 2(b), the band dispersion of the Dirac cone is insensitive to the change of photon energy (19 and 51 eV) in the heavily Cu-doped sample ($x = 0.25$) as well as in pristine Bi_2Se_3 [see Fig. 1(c)], indicating that the Cu doping does not alter the surface nature of the band. Figure 2(c) shows the comparison of band dispersion near E_F for four different samples of $x = 0.0-0.25$, where each band dispersion is shifted so as to align the Dirac point at the same energy. As clearly visible, all band dispersions from different samples overlap very well, demonstrating that the Cu doping

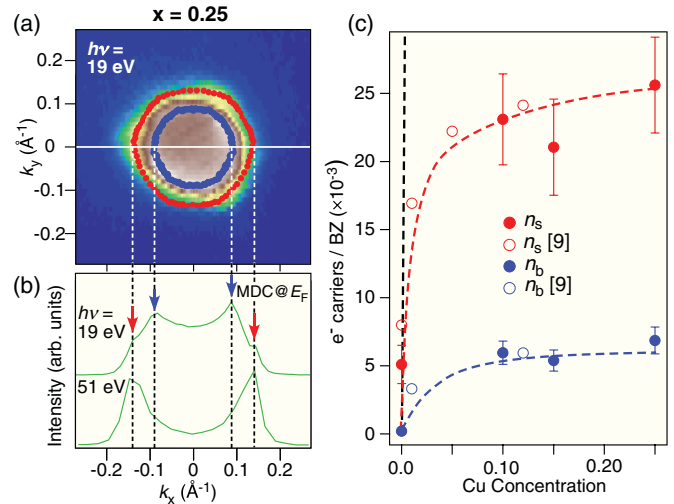


FIG. 3. (Color online) (a) ARPES intensity map at E_F of $\text{Cu}_x\text{Bi}_2\text{Se}_3$ ($x = 0.25$) as a function of two-dimensional wave vector measured at $h\nu = 19$ eV. The intensity at E_F has been obtained by integrating the ARPES spectra within ± 5 meV with respect to E_F . Red and blue circles show experimental Fermi vectors (k_F 's) of the surface and bulk conduction bands, respectively, estimated by tracing the peak maxima in the momentum distribution curves (MDCs). The k_F points were folded by taking into account the crystal symmetry. (b) MDCs at E_F of $\text{Cu}_x\text{Bi}_2\text{Se}_3$ ($x = 0.25$) measured at $h\nu = 19$ and 51 eV. Dashed lines in (a) and (b) correspond to the momentum location of k_F points along the k_x axis. (c) Cu doping dependence of the bulk and surface carrier numbers with respect to each Brillouin zone (n_b and n_s). Filled circles are obtained from the present ARPES experiment and open circles are from a previous study.⁹ The black dashed line represents the theoretical x dependence of carrier concentrations when one assumes that all the doped Cu atoms are intercalated into the van der Waals gap between Bi_2Se_3 quintuple layers to produce one electron per one Cu atom. Red and blue dashed lines are guides for the eyes to trace the x dependence of n_s and n_b , respectively.

does not alter the shape of band dispersion, but simply induces a rigid-band-like shift of band dispersions.

To evaluate the bulk and surface carrier concentrations as a function of the Cu concentration, we have estimated the Fermi vector (k_F) from the momentum distribution curves (MDCs) at E_F as shown in Figs. 3(a) and 3(b). The MDC at E_F along k_x axis at $h\nu = 19$ eV consists of two sets of double peaks corresponding to the k_F points of the surface state (red arrows) and the bulk CB (blue arrows). It is remarked that the bulk component is totally absent at $h\nu = 51$ eV, while the surface k_F points are more clearly seen in the same MDC. Figure 3(c) shows the estimated surface and bulk carrier concentrations (n_s and n_b) as a function of Cu doping. In the estimation, we assumed a two-dimensional (2D) cylindrical Fermi surface for n_s , while for n_b we took into account the 3D nature of the bulk Fermi surface determined by photon-energy-dependent ARPES.⁹ As seen in Fig. 3(c), both n_s and n_b rapidly increase with Cu doping in the early stage of doping ($0.0 \leq x \leq \sim 0.05$), while they show a tendency to saturate on further doping and keep almost constant at $x > 0.1$, as expected from the experimental results for the chemical potential shift shown in Fig. 2(a). The observed saturation of n_b is consistent with

a recent transport study reporting that the bulk carrier number estimated with the Hall coefficient remains almost constant in a wide x range of heavy doping ($0.14 \leq x \leq 0.4$).¹³ The current ARPES result, which also demonstrates the saturation of n_s , thus establishes that the carrier saturation behavior is a common feature of both bulk and surface.

We notice that the estimated n_b is much smaller than that expected from the simple Cu intercalation picture where one doped Cu atom donates one electron to the parent material Bi_2Se_3 . For example, as seen in Fig. 3(c), the actual carrier concentration at $x = 0.1$ ($n_b = 0.005$) shows a sharp contrast to the simple theoretical value ($n_b = 0.1$), suggesting the ambipolar nature of doped Cu atoms,^{9,10,13} i.e., both the electron and hole doping simultaneously take place upon Cu doping. In fact, previous transport and crystallographic studies of Cu-doped Bi_2Se_3 ^{8,13} suggested that Cu intercalation causes electron doping while hole doping also takes place when a Bi atom is substituted with a Cu atom.^{13,21} All these results, along with the present ARPES study, suggest that the total carrier concentration in Cu-doped Bi_2Se_3 is dominated by a subtle balance between the competing two processes originating in the local structure of doped Cu atoms. It is inferred from the present ARPES results that Cu atoms are predominantly intercalated in the early stage of doping ($x < 0.05$), while the substitution of Cu for Bi increases on further doping, resulting in the saturation of the carrier concentration.

Next we discuss the superconductivity in $\text{Cu}_x\text{Bi}_2\text{Se}_3$ based on the present ARPES results. Our magnetic susceptibility measurements indicate that superconductivity emerges between $x = 0.10$ and 0.12 , where the chemical potential and the carrier concentration start to saturate [see Figs. 2(a) and 3(c)]. This suggests that the observed carrier saturation and the emergence of superconductivity are closely related to each other. Moreover, the T_c value, as determined by magnetic susceptibility measurements, is reported to be insensitive to the

Cu concentration above $x > 0.12$.¹³ This is in good accordance with the carrier saturation behavior observed in the present ARPES study.

Finally, we briefly comment on the topological aspects of the present ARPES results. As seen in Fig. 1(d), the surface state persists even in the heavily Cu-doped region of $x = 0.25$, indicating that the topological surface state in $\text{Cu}_x\text{Bi}_2\text{Se}_3$ is substantially robust against scattering by doped Cu atoms. Such a peculiar nature of the surface state may be useful for realizing novel TSC/TI devices used for quantum computation^{22,23} because the performance of these devices would rely on the robustness against the doping variation and disorders in the crystal.

IV. SUMMARY

We have reported high-resolution ARPES results of Cu-doped topological insulator Bi_2Se_3 for a wide range of doping ($x = 0.0$ – 0.25). We observed that both the bulk and surface carrier concentrations exhibit an unexpected saturation at $x \sim 0.1$ in the successive Cu doping up to $x = 0.25$. This doping level ($x \sim 0.1$) coincides with the doping level where superconductivity emerges, suggesting a close relationship between the carrier saturation and the emergence of superconductivity. We have also revealed that the topological surface state persists even in the heavily doped region of $x = 0.25$, suggesting its robustness against doping and impurities.

ACKNOWLEDGMENTS

This work was supported by grants from JST-CREST, JSPS, MEXT of Japan and MOST, CAS, NSFC of China. This work is based in part upon research conducted at the Synchrotron Radiation Center, which is primarily funded by the University of Wisconsin-Madison with supplemental support from facility users and the University of Wisconsin-Milwaukee.

¹M. Z. Hasan and C. L. Kane, *Rev. Mod. Phys.* **82**, 3045 (2010).

²X.-L. Qi and S.-C. Zhang, *Rev. Mod. Phys.* **83**, 1057 (2011).

³Y. Xia, D. Qian, D. Hsieh, L. Wray, A. Pal, H. Lin, A. Bansil, D. Grauer, Y. S. Hor, R. J. Cava, and M. Z. Hasan, *Nat. Phys.* **5**, 398 (2009).

⁴S. Souma, K. Kosaka, T. Sato, M. Komatsu, A. Takayama, T. Takahashi, M. Kriener, K. Segawa, and Y. Ando, *Phys. Rev. Lett.* **106**, 216803 (2011).

⁵P. Roushan, J. Seo, C. V. Parker, Y. S. Hor, D. Hsieh, D. Qian, A. Richardella, M. Z. Hasan, R. J. Cava, and A. Yazdani, *Nature (London)* **460**, 1106 (2009).

⁶J. Seo, Pedram Roushan, H. Beidenkopf, Y. S. Hor, R. J. Cava, and A. Yazdani, *Nature (London)* **466**, 343 (2010).

⁷C. L. Kane and E. J. Mele, *Science* **314**, 1692 (2006).

⁸Y. S. Hor, A. J. Williams, J. G. Checkelsky, P. Roushan, J. Seo, Q. Xu, H. W. Zandbergen, A. Yazdani, N. P. Ong, and R. J. Cava, *Phys. Rev. Lett.* **104**, 057001 (2010).

⁹L. A. Wray, S. Xu, Y. Xia, Y. S. Hor, D. Qian, A. V. Fedorov, H. Lin, A. Bansil, R. J. Cava, and M. Z. Hasan, *Nat. Phys.* **6**, 855 (2010).

¹⁰L. A. Wray, S. Xu, Y. Xia, D. Qian, A. V. Fedorov, H. Lin, A. Bansil, L. Fu, Y. S. Hor, R. J. Cava, and M. Z. Hasan, *Phys. Rev. B* **83**, 224516 (2011).

¹¹P. Das, Y. Suzuki, M. Tachiki, and K. Kadowaki, *Phys. Rev. B* **83**, 220513(R) (2011).

¹²M. Kriener, K. Segawa, Z. Ren, S. Sasaki, and Y. Ando, *Phys. Rev. Lett.* **106**, 127004 (2011).

¹³M. Kriener, K. Segawa, Z. Ren, S. Sasaki, S. Wada, S. Kuwabata, and Y. Ando, *Phys. Rev. B* **84**, 054513 (2011).

¹⁴S. Sasaki, M. Kriener, K. Segawa, K. Yada, Y. Tanaka, M. Sato, and Y. Ando, *Phys. Rev. Lett.* **107**, 217001 (2011).

¹⁵L. Fu and E. Berg, *Phys. Rev. Lett.* **105**, 097001 (2010).

¹⁶M. Sato, *Phys. Rev. B* **81**, 220504 (2010).

¹⁷M. Sato, Y. Takahashi, and S. Fujimoto, *Phys. Rev. B* **82**, 134521 (2010).

- ¹⁸M. Bianchi, D. Guan, S. Bao, J. Mi, B. B. Iversen, P. D. C. King, and Ph. Hofmann, *Nat. Commun.* **1**, 128 (2010).
- ¹⁹L. A. Wray, S. Xu, M. Neupane, Y. Xia, D. Hsieh, D. Qian, A. V. Fedorov, H. Lin, S. Basak, Y. S. Hor, R. J. Cava, A. Bansil, and M. Z. Hasan, e-print [arXiv:1105.4794](https://arxiv.org/abs/1105.4794).
- ²⁰H. M. Benia, C. Lin, K. Kern, and C. R. Ast, *Phys. Rev. Lett.* **107**, 177602 (2011).
- ²¹J. Bludská, S. Karamazov, J. Navrátil, I. Jakubec, and J. Horáček, *Solid-State Ionics* **171**, 251 (2004).
- ²²L. Fu and C. L. Kane, *Phys. Rev. Lett.* **100**, 096407 (2008).
- ²³A. Y. Kitaev, *Ann. Phys. (NY)* **303**, 2 (2003).